理 學 碩 士 學 位 論 文

Studies on Shape-Controlled Nanoparticles for Enhanced Electrocatalytic Reaction

(전기화학 촉매 반응 활성 향상을 위한

형상이 조절된 나노 입자 연구)

蔚 山 大 學 校 大 學 院

化 學 科

劉 智 恩

Studies on Shape-Controlled Nanoparticles for Enhanced Electrocatalytic Reaction

指 導 敎 授 홍 종 욱

指 導 敎 授 정 재 훈

이 論文을 理學碩士 學位 論文으로 제출함

2024年 02月

蔚 山 大 學 校 大 學 院

化 學 科

劉 智 恩

劉 智 恩의 理學碩士 學位 論文을 認准함

蔚 山 大 學 校 大 學 院

2024年 02月

국문요약

화석연료로 인한 환경오염 문제가 심각해지고, 자원 고갈 위기에 맞아 새로운 에너지에 대한 연구 필요성은 이전보다 대두되고 있다. 새로운 에너지는 지속 가능한 미래를 위한 형태를 띄고 있어야 하기에 풍부한 자원을 활용하고, 환경 오염을 최소화할 필요가 있다. 이러한 관점에서 전기화학을 통한 에너지 전환은 물, 산소, 수소, 이산화탄소 등 풍부한 자원을 이용해 이루어지기에 이는 재생가능한 에너지원으로 유망하다. 전기화학을 통한 에너지 전환의 종류에는 수소 생산, 산소 환원, 알코올 산화와 같은 연료전지 반응과 이산화탄소의 환원에 의한 탄화수소 생산을 포함하여 다양한 반응들이 있다.

이러한 전기화학 반응에 필요한 활성화 에너지를 낮추고 전체 반응의 효율을 향상시키기 위해서는 전극에 사용되는 촉매가 중요하다. 촉매의 표면에서 전기화학 반응이 빠르게 일어나기 위해서는 반응물과 촉매 사이의 흡착 세기가 조절되어야 한다. 반응물이 촉매 표면에 원활하게 흡착하여 반응하고 난 뒤에 생성물로 전환되어 쉽게 떨어져야하기 때문이다. 따라서 촉매와 반응물 사이의 흡착 특성을 조절하는 것은 촉매 연구에서 중요한 부분이며 이를 달성하기 위해 다양한 형태의 합금과 형상 조절이 필요하다. 합금을 통해서는 구성 성분간 전기음성도 차이, 격자상수 차이 등에 의해 전자구조의 변화를 유도할 수 있으며 변화된 전자구조에 의해 흡착물과의 흡착 특성이 변화할 수 있다. 또한 형상 조절을 통해 표면 원자 구조에 변화가 생기면 표면 원자의 배위수가 줄어듦에 따라 반응물과의 흡착특성 변화가 가능하다.

촉매의 활성은 위와 같이 반응물과 촉매 사이 흡착 특성 조절을 통해 이룰 수 있으며 또 다른 방법은 활성 부위를 증가시키는 것이다. 촉매의 활성 부위를 증가시키기 위해서 촉매 자체의 형상 조절을 통해 부피 대 표면적을 극대화할 수 있다. 나노시트와 같은 이차원 구조나 다공성 구조로 촉매를 디자인함으로써 원자의 활용성을 극대화하고 반응물과 생성물의 빠른 이동을 유도함으로써 촉매의 활성을 증가시킬 수 있는 것이다.

이 논문에서는 형상 및 합금의 조성 조절을 통해서 촉매를 합성하고 전기화학 반응에 활용하였다. 이를 통해서 촉매의 형상 및 조성이 전기화학적 활성에 큰 영향을 미치는 것을 확인할 수 있었다.

Abstract

The increasing environmental pollution resulting from fossil fuel usage and the looming threat of resource depletion have heightened the need for research into alternative energy sources. From this perspective, electrochemical energy conversion, using abundant resources such as water, oxygen, hydrogen, and carbon dioxide, emerges as a promising avenue for sustainable energy production. Various electrochemical reactions fall under this category, including hydrogen production, oxygen reduction, alcohol oxidation in fuel cells, and carbon dioxide reduction for hydrocarbon generation.

To enhance the efficiency and reduce the activation energy required for these electrochemical reactions, the choice of catalysts used at the electrodes becomes crucial. For efficient electrochemical reactions, it is essential that reactants are adequately adsorbed on the catalyst's surface, facilitating rapid reactions, followed by the easy release of the products. Therefore, controlling the adsorption characteristics between catalyst and reactants is a pivotal aspect of catalyst research. Achieving this necessitates the utilization of different forms of catalysts, including alloys and shape manipulation.

Alloys can induce changes in electronic structure due to differences in electronegativity between their components and lattice constants, thereby altering the adsorption characteristics of the catalyst surface. Furthermore, by manipulating the catalyst's shape, changes in the surface atomic structure can be achieved, allowing for adjustments in adsorption properties as the coordination number of surface atoms is reduced.

Modulating the adsorption characteristics between reactants and catalysts, as described above, contributes to enhancing catalyst activity. Another approach involves increasing the active sites of the catalyst by controlling its shape. By controlling the morphology of catalyst, it is possible to maximize the surface area relative to its volume, thus augmenting its catalytic activity. Designing catalysts with two-dimensional structures like nanosheets or porous structures maximizes the utilization of atoms and enhances the catalytic activity by facilitating rapid movement of reactants and products.

In this paper, we synthesized catalysts by controlling both shape and alloy composition and applied them to electrochemical reactions. Through these experiments, we confirmed that the shape and composition of the catalyst significantly impact its electrochemical activity.

In summary, electrochemical energy conversion, driven by catalyst research involving adsorption control and the augmentation of active sites through shape manipulation and alloy

composition, offers great promise as a sustainable energy source, particularly in the context of mitigating environmental pollution and addressing resource scarcity.

Index

Korean abstract ····· iv

Abstract ····· vi

I. Introduction ····· 9

II. Experimental ····· 11

III. Results and Discussion ····· 13

IV. Conclusion ····· 31

V. References ····· 32

I. Introduction

In recent years, fuel cells based on the electrochemical oxidation of small organic molecules have garnered increased attention due to their high energy/power density and the ease of storing and delivering liquid fuels. [1] Among various fuel cell systems, direct ethanol fuel cells (DEFCs) stand out as particularly intriguing. [1-3] This is primarily attributed to low toxicity and abundance of ethanol. However, despite their immense potential, the development of DEFCs has faced challenges, primarily the need for highly active and durable electrocatalysts for the ethanol oxidation reaction (EOR) at the anode. Pt-based electrocatalysts have been extensively investigated for their exceptional ability to catalyze fuel oxidation. [4-6] However, the scarcity of Pt and its limited durability have spurred significant interest in developing alternative electrocatalysts. To address these limitations, extensive efforts have been dedicated to minimizing electrocatalyst loading and enhancing Pt utilization efficiency through morphology and composition control. [4, 5] The alloying of Pt with suitable auxiliary metals has emerged as a promising approach, enhancing electrocatalytic performance while simultaneously reducing the required electrocatalyst loading. Among various Pt-based bimetallic alloys, Pt-Pd alloys have demonstrated outstanding electrocatalytic performance across a wide range of electrochemical reactions, including small molecule oxidation such as EOR, owing to their precisely controlled electronic structures. [7-9] On the other hand, the incorporation of oxophilic metals into Pt materials has proven effective in enhancing EOR activity. This enhancement is attributed to their ability to readily form surface-adsorbed hydroxides ($(OH)_{ads}$), which accelerate the electrochemical oxidation of adsorbed intermediates such as $(CO)_{ads}$ and $(CH_3CO)_{ads}$. [10, 11]

Ultrathin two-dimensional (2D) metal nanosheets (NSs) are of extraordinary fascination in catalytic regions, because they exhibit high atomic utilization efficiency due to high surface-to-volume ratios by their thin thickness. In addition to morphological advantages of ultrathin metal NSs, porous edged ultrathin metal NSs are a rare class of nanostructures with high morphological anisotropy. These NSs can offer large surface areas and rich undercoordinated surface atoms, can offer an effective platform for exploring the catalytic function of low-coordinated surface and may hold unexpected promise for catalytic applications. Despite their high potential as an efficient electrocatalyst, the synthesis of metal NSs has encountered limitations due to three-dimensional (3D) growth of metals that possess face-centered cubic crystal structures. A noteworthy approach introduced by Huang et al. involved the utilization of carbon monoxide (CO) as a surface stabilizer on the basal plane of Pd nanostructures, yielding ultrathin Pd NSs with a thickness of 1.8 nm. [12]

Subsequently, various Pd-based ultrathin NSs, including Pd, PdAg, PdNi, PdCu, and PdPtAg NSs, were reported based on CO-mediated synthesis. [13-16] However, the strong bonding strength of CO on Pd surface can hinder the adsorption of reagents and further progress for electrocatalysis. Although amines have been sporadically employed in the synthesis of 2D nanostructures, although amines have sporadically played a role in the synthesis of 2D nanostructures, the realm of extended ultrathin nanosheets remained largely unexplored without the employment of CO. [17] Moreover, the intricate syntheses of these nanosheets limits their industrial applications. Consequently, the pursuit of metal NSs with highly porous edges in the absence of strong surface binding stabilizers poses a formidable challenge.

In this study, we present the facile synthesis approaches for three types of ternary alloy ultrathin PdAg/PtPdAg NSs with highly porous edges (PdAg/PtPdAg P-NSs). The PdAg/PtPdAg P-NSs were synthesized under mild reduction condition and in absence of strong surface binding stabilizer, resulting in the creation of fresh active sites. The PdAg/PtPdAg P-NSs with a 1:1:1 atomic ratio of Pd/Pt/Ag comprise a PdAg alloy central basal plane and highly porous PtPdAg alloy edges, resulting in a high surface-to-volume ratio due to their atomic-thin thickness and abundant undercoordinated atoms at the porous edges. As the Pd atomic ratio increases within the Pd/Pt/Ag composition of the NSs, a reduction in edge porosity is observed. Consequently, PdAg/PtPdAg NSs composed of rounded edges (R-NSs) with a 5:1:1 atomic ratio of Pd/Pt/Ag and PdAg/PtPdAg 3D nanocrystals (3D-NCs) with a 10:1:1 atomic ratio of Pd/Pt/Ag exhibit progressively diminished edge porosities.

Thanks to the large active sites associated with ultrathin thickness, abundant undercoordinated atoms, and oxophilic Ag atoms on the surface, the PdAg/PtPdAg P-NSs exhibited impressively high EOR activity compared to different NSs, up to 10 times higher than commercial Pd/C. In addition, the different edge porosities of the NSs allowed to investigate for correlation between undercoordinated atoms at the porous edges and electrocatalytic performance for EOR. This current synthesis approach paves the way for the design and development of advanced highly porous multimetallic 2D electrocatalysts, opening up possibilities for a wide range of valuable applications.

II. Experimental

Chemicals and materials. Potassium chloride (ll) ($PdCl_2$, ≥99%), potassium tetrachloroplatinate (ll) (K_2PtCl_4, 98%), silver nitrate ($AgNO_3$, ≥99.0%), octadecyl trimethyl ammonium chloride (OTAC, ≥ 95%), 2-propanol (IPA, ≥ 99.5 %), and nafion ® perfluorinated resin solution (5 wt%) were purchased from Sigma-Aldrich, Palladium on activated carbon (Pd/C, 20 wt%), and L-ascorbic acid (AA, 99.0%) were obtained from Alfa aesar. Potassium hydroxide (KOH, 95.0%) from Samchun, and Hydrochloric acid from Duksan (HCl, 35~37%) is used. Ethyl alcohol anhydrous (ethanol, ≥ 99.9 %) from Daejung is used. Deionized water with a resistivity of greater than 18.3 MΩ·cm was used in the preparation of reaction solutions.

Synthesis of PdAg/PtPdAg nanosheets. To synthesize PdAg/PtPdAg P-NSs, 0.5 mL of 20 mM H_2PdCl_4, 1 mL of 10 mM K_2PtCl_4, and 1 mL of 10 mM $AgNO_3$ is added to 10 mM OTAC aqueous solution will be sonicated for 30 minutes. After sonication, 1.5 mL of 0.2 M Ascorbic acid will be injected into the solution. The reaction solution is kept at 20 °C for 2 hours. The color of the solution containing nanosheets changes to black. By centrifugation at 10000 rpm for 10 minutes, Nanosheets can be obtained. PdAg/PtPdAg R-NSs and 3D-NCs can be synthesized by adjusting the volume of the H_2PdCl_4 to 2.5 mL and 5 mL.

Characterization. The morphology of PdAg/PtPdAg nanosheets and nanocrystals were characterized by scanning electron microscopy (SEM) on JEOL JEM-7210F and transmission electron microscopy (TEM) on JEOL JEM-2100F. The Pd:Ag:Pt atomic ratio was analyzed by using Spectroblue-ICP-OES (Ametek) and HAADF-STEM-EDS. To investigate the crystal structure, X-ray diffraction patterns (XRD) were obtained on a Rigaku D/MAX2500V/PC scanning for 2θ at 20 to 90 degrees. X-ray photoelectron spectroscopy (XPS) is conducted on ThermoFisher K-alpha.

Electrochemical measurements.

Electrochemical experiments were performed in a three-electrode cell by using EC-Lab Biologic Model SP-300 potentiostat in alkaline condition. Graphite and Hg/HgO (1 M NaOH) were used as the counter and the reference electrodes, respectively.

Working electrode is prepared as following method. 5 μL of the catalyst ink containing 2 μg of Pd and Pt onto a glassy carbon electrode (GCE, diameter: 5 mm), and then dried. The prepared GCE was used as working electrode and is cleaned electrochemically by 20 cycles between -0.845 V and 0.250 V *vs.* Hg/HgO at a scan rate of 50 mV s^{-1} in 1.0 M KOH that purged with N_2 gas for 30 min before electrochemical experiment. The CVs of PdAg/PtPdAg NSs and 3D NCs, Pd/C were obtained from -0.845 V to 0.250 V *vs.* Hg/HgO at a scan rate of 50 mV s^{-1} in 1.0 KOH + 1.0 M ethanol.

III. Result and Discussion

Figure 1a shows a Transmission Electron Microscopy (TEM) image of synthesized PdAg/PtPdAg P-NSs, showing formation of the 2D nanostructures with porous edges and an average diameter of 40.99 ± 5.0 nm. In **Figure 1b**, TEM image of the PdAg/PtPdAg P-NSs showed the porous edges including undercoordinated step atoms, which can be active sites for small molecule oxidation/reduction reactions. The d-spacing for adjacent lattice fringes of PdAg/PtPdAg P-NSs was determined to 2.29 Å well matched with (111) plane of the fcc PdAg and PtPdAg alloys. [16] To check the thickness of the PdAg/PtPdAg P-NSs, TEM image of side face of the PdAg/PtPdAg P-NSs was obtained, which exhibit the atomic thin thickness of 3.21±0.6 nm **(Figure 1c)**. To investigate the compositional structure of PdAg/PtPdAg P-NSs, we carried out HAADF-STEM and corresponding energy dispersive X-ray spectroscopy (EDS) measurements on the PdAg/PtPdAg P-NSs. In the central region of the PdAg/PtPdAg P-NSs, Pd and Ag signals were observed in entire NSs, whereas Pt signals were intensively detected at porous edge regions **(Figure 1d)**. These indicate that PdAg/PtPdAg P-NSs are composed of PdAg alloy central region/PtPdAg porous edges. This structure can be attributed to the later reduction of Pt compared to Pd and Ag, as Pt forms stable complexes with halides in the presence of halides. The XRD pattern of the PdAg/PtPdAg P-NSs shows that all diffraction peaks appeared between those of Pd/Pt and Ag references, further demonstrating the formation of alloy compositions **(Figure 1e)**.

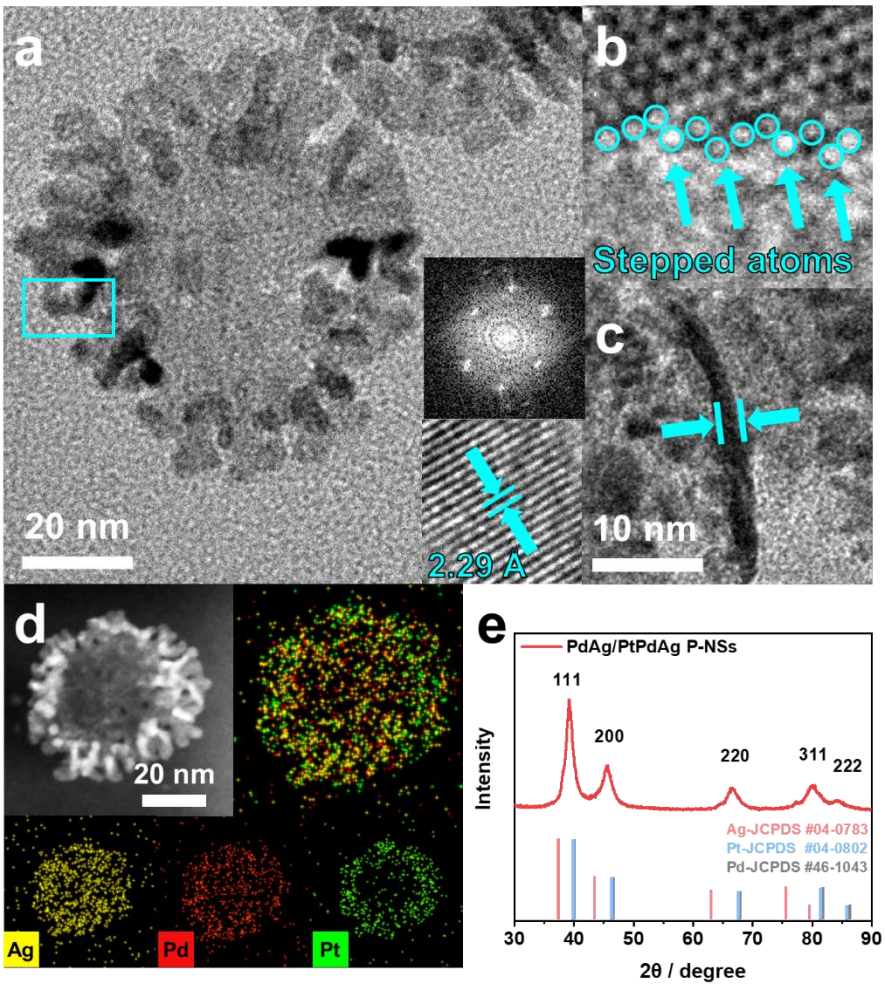

Fig. 1 a) Low-magnification TEM image of PdAg/PtPdAg P-NSs (lattice fringes and FFT patterns are shown in the insets). b) TEM image of region inside the blue rectangle in 1a shows the atoms on NSs. c) TEM image of side face of PdAg/PtPdAg P-NSs. d) HAADF STEM image and corresponding EDS elemental maps of a PdAg/PtPdAg P-NS. e) XRD patterns of PdAg/PtPdAg P-NSs.

It is noteworthy to emphasize that the final morphology of the NSs strongly correlates with the quantity of H_2PdCl_4 used as the Pd precursor. As depicted in the STEM and TEM images **(Figure 2)**, three distinct nanostructures are formed when varying amounts of H_2PdCl_4 are used under otherwise identical synthesis conditions. When 2.5 mL of H_2PdCl_4 (20 mM) was employed in the synthesis, deviating from the 0.5 mL used in the standard procedure, NSs with rounded and lumpy edges were generated, with a lateral size of 65.71 ± 9 nm **(Figure 2b, e)**. The bulk Pd/Pt/Ag atomic ratio, as determined by EDS, was 67.6:15.9:16.5. Increasing the quantity of H_2PdCl_4 to 5 mL resulted in quasi-spherical NCs with an average lateral size of 77.65 ± 9 nm and bulk Pd/Pt/Ag atomic ratio of 79.8:10.0:10.2 **(Figure 2c, f)**. The products formed by using 2.5 and 5 mL of H_2PdCl_4 (20 mM) exhibited typical fcc crystal structure confirmed by XRD measurement **(Figure 3)**. These findings indicated that with the increasing Pd content, the suppression of out-of-plane growth in the 2D NSs is weaken, leading to the formation of 3D nanostructures with larger lateral dimensions. Among them, PdAg/PtPdAg P-NSs has the smallest size and an ultrathin 2D structure, suggesting that it may possess higher electrochemical activity compared to the other particles.

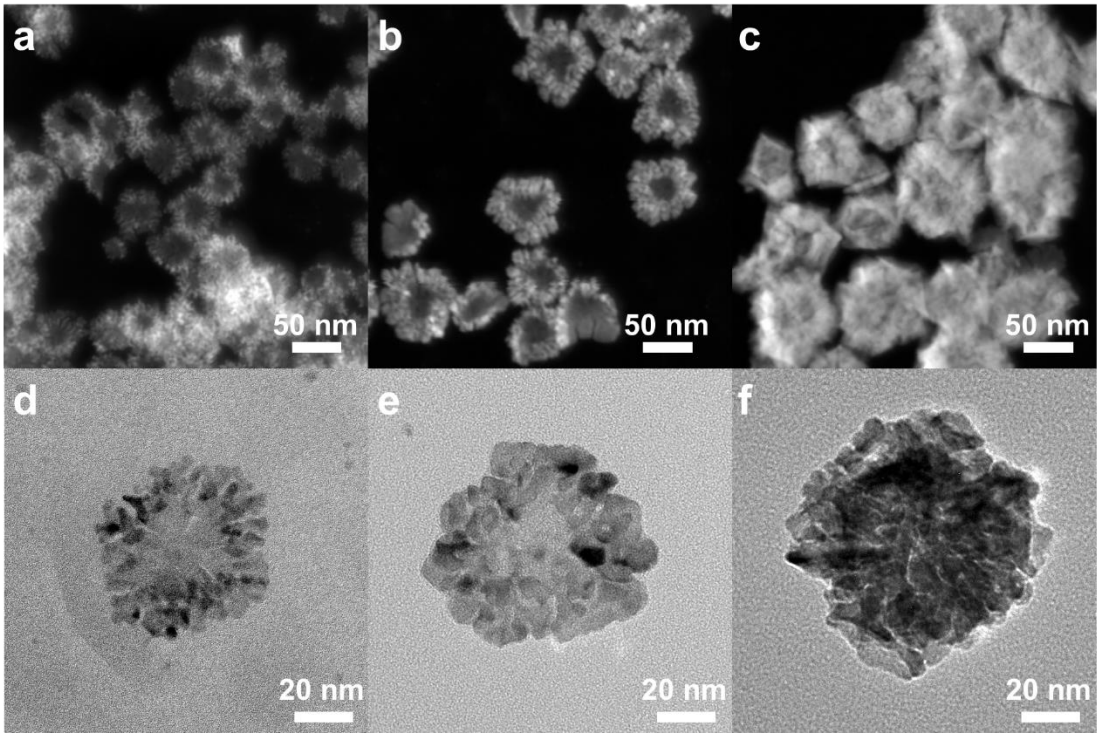

Fig. 2 a), d) STEM and low-magnification TEM images of PdAg/PtPdAg P-NSs. b), e) STEM and low-magnification TEM images PdAg/PtPdAg R-NSs. c, f) STEM and low magnification images of PdAg/PtPdAg 3D-NCs.

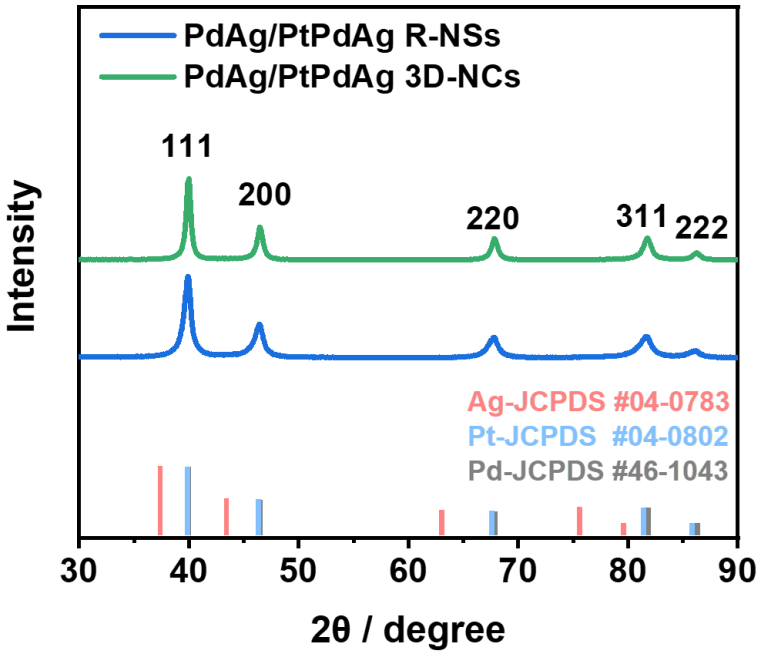

Fig. 3 XRD patterns of PdAg/PtPdAg P-NSs, PdAg/PtPdAg R-NSs, and PdAg/PtPdAg 3D-NCs.

To investigate the influence of OTAC and AA during the synthesis of the NSs, various concentrations of OTAC-containing reaction mixtures were prepared while keeping other synthesis conditions unchanged. The scanning electron microscopy (SEM) image of the particles is shown in **Figure 4**. When using a higher concentration of OTAC, specifically 20 mM, smaller-sized sheets were synthesized, but they exhibited irregular shapes due to aggregation between the sheets. At lower concentrations of OTAC, particles in a 3D form rather than 2D sheets were synthesized. As the concentration of OTAC decreased, the particles became more spherical in shape, and their size increased. These results suggest that at lower concentrations, the lack of OTAC results in a rapid reduction of metal ions and uncontrolled particle shaping. Furthermore, since OTAC is used as a template for synthesizing nanoparticles, a lower amount of OTAC would lead to fewer seed particles, resulting in the growth of larger-sized particles.

Experiments were also conducted by adjusting the volume of the AA solution. The SEM images of the nanoparticles obtained accordingly are shown in **Figure 5**. When a larger amount of AA was used, the high reduction power led to the rapid reduction of metal ions, resulting in the synthesis of particles that attached to the NSs in the form of small particles. However, at lower concentrations, irregularly shaped nanoparticles were produced due to the poor reduction power.

Furthermore, it was anticipated that temperature would be a critical factor in the synthesis of the NSs, and to confirm this, temperature control experiments were conducted. Experiments were carried out at temperatures of 10 °C, 30 °C, 40 °C, in addition to the standard condition of 20 °C, and the results are presented in **Figure 6**. At lower temperature, the reduction rate was consistently lower, resulting in the formation of a two-dimensional shape, though without porous edge structures. Conversely, at higher reaction temperatures, the reduction rates among metal precursors increased, indicating the formation of three-dimensional particle shapes.

By adjusting the molar ratio of metals, the concentration of OTAC, and the volume of AA, we were able to synthesize PdAg/PtPdAg P-NSs with optimal conditions that exhibit ultrathin characteristics and dendritic edges, resulting in a high surface area. We expect that these particles will demonstrate high electrocatalytic activity.

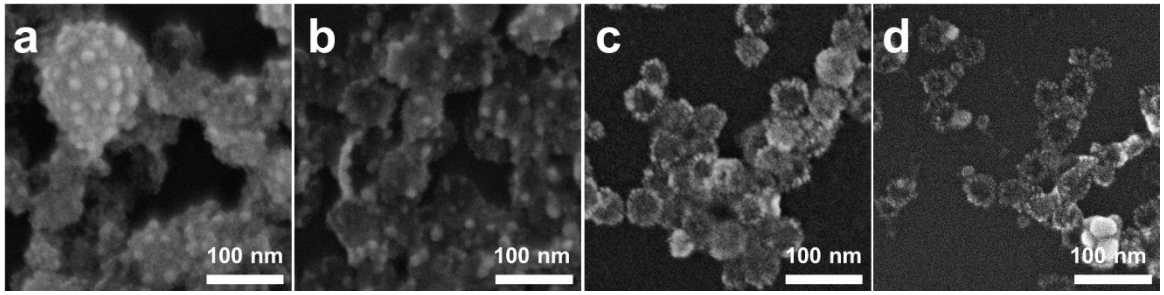

Fig. 4 PdAg/PtPdAg nanoparticles synthesized in 20 mL of a) 1 mM OTAC, b) 3 mM OTAC, c) 10 mM OTAC, and d) 20 mM OTAC.

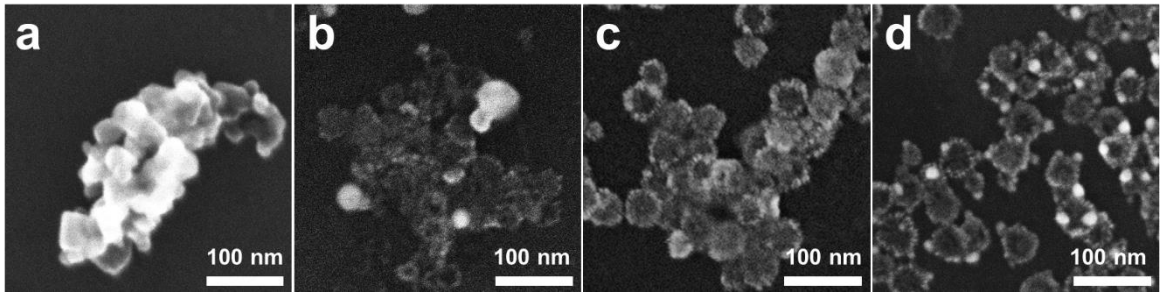

Fig. 5 PdAg/PtPdAg nanoparticles synthesized in a) 0.05 mL, b) 0.25 mL, c) 0.15 mL, and d) 2.50 mL of 0.2 M AA.

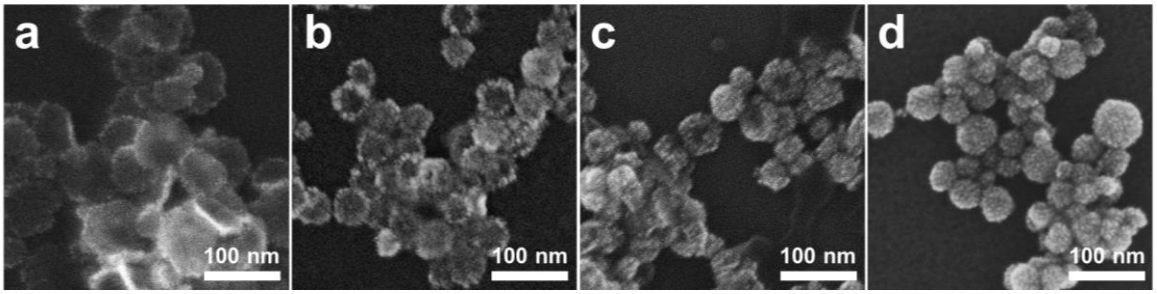

Fig. 6 PdAg/PtPdAg nanoparticles synthesized a) 10 °C, b) 20 °C, c) 30 °C, and d) 40 °C.

To investigate the electronic structure of the PdAg/PtPdAg P-NSs, X-ray photoelectron spectroscopy (XPS) measurement was performed and compared with those of PdAg/PtPdAg R-NSs and PdAg/PtPdAg 3D-NCs. In the Pd 3d and Pt 4f core-level XPS spectra of the PdAg/PtPdAg P-NSs, there were discernible shifts to lower binding energies relative to the spectra of PdAg/PtPdAg R-NSs and PdAg/PtPdAg 3D-NCs, whereas the binding energies for Ag 3d exhibited an increase **(Figure 7)**. This observed trend can be rationalized by electron migration from Ag to both Pt and Pd within the PdAg/PtPdAg P-NSs. Owing to this electron transfer, the d-band center of Pt and Pd can be effectively shifted downwards. This lowered d-band center of Pd and Pt facilitates an enhanced interaction with the p orbitals of O in $(OH)_{ads}$, which plays a crucial role in promoting the efficient carbonaceous poisoning adsorbates such as $(CO)_{ads}$.

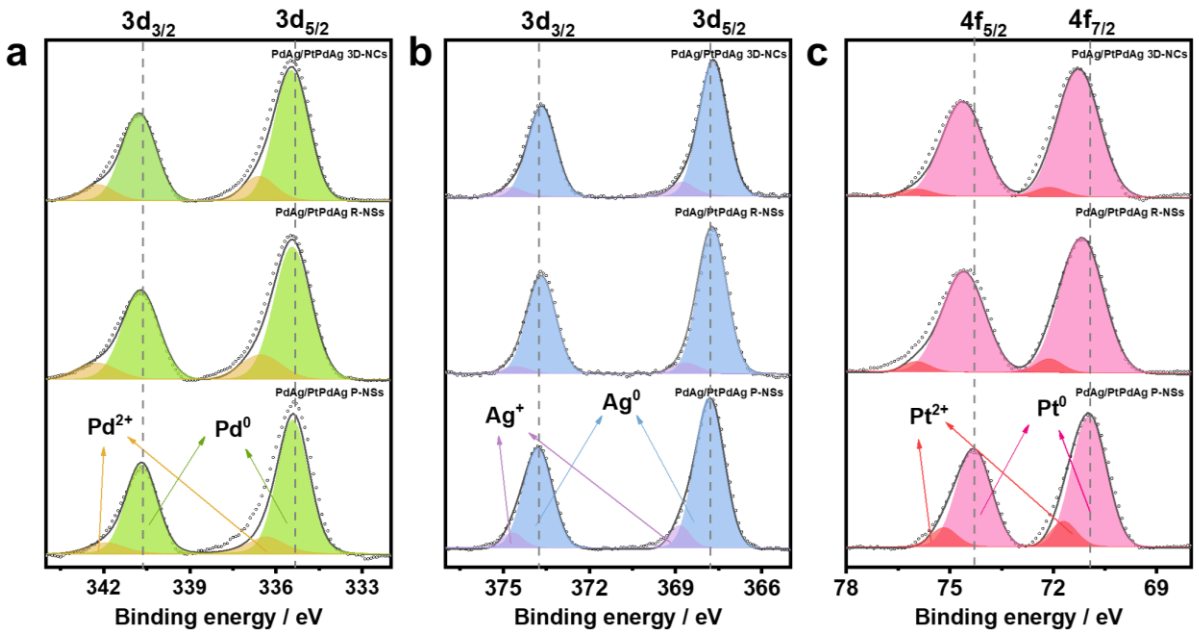

Fig. 7 XPS spectra of a) Pd b) Ag and c) Pt in PdAgPt P-NSs, R-NSs, and 3D-NCs.

To gain insight into the influence of the morphology and composition of the PdAg/PtAdAg P-NSs on electrocatalytic performance, we investigated electrocatalytic properties of PdAg/PtPdAg P-NSs, PdAg/PtAdAg R-NSs, PdAg/PtAdAg 3D-NCs, and commercial Pd/C catalysts for EOR. The PdAg/PtPdAg P-NSs, PdAg/PtAdAg R-NSs, and PdAg/PtAdAg 3D-NCs were loaded onto a carbon support (C, Vulcan XC-72R). **Figure 8a** displays the cyclic voltammograms (CVs) of these various catalysts obtained in N_2-saturated 1.0 M KOH. The electrochemically active surface areas (ECSAs) of the catalysts were estimated based on the columbic charge generated by reduction of oxygen species adsorbed on the working electrode in a potential range from -0.845 to 0.250 V vs. Hg/HgO reference electrode. The ECSAs for PdAg/PtPdAg P-NSs, PdAg/PtPdAg R-NSs, PdAg/PtPdAg 3D-NCs, and Pd/C were 38.17, 25.92, 16.08, and 37.97 $m^2 g^{-1}$, respectively, indicating a higher metal utilization efficiency of the PdAg/PtPdAg P-NSs compared to other catalysts. In addition, these results revealed that transformation from the ultrathin thickness of 2D PdAg/PtPdAg P-NSs to the 3D morphology of PdAg/PtPdAg 3D-NCs leads to a decrease in ECSAs.

To evaluate the electrocatalytic activity of the catalysts toward EOR, CVs were obtained in 1.0 M KOH including 1.0 M ethanol. The mass activity of the catalysts was determined by normalizing their current density to the mass of metal loaded on a glassy carbon electrode (GCE). As shown in **Figure 8b**, PdAg/PtPdAg P-NSs exhibited a remarkable mass activity of 10.44 A mg^{-1}, which was 2.5, 6.4, and 6.6 times higher compared to that of PdAg/PtPdAg R-NSs (4.20 A mg^{-1}), PdAg/PtAdAg 3D-NCs (1.63 A mg^{-1}), and Pd/C (1.58 A mg^{-1}), respectively. Furthermore, the onset potential of PdAg/PtPdAg P-NSs measured at 0.15 A mg^{-1} was -0.543 V, representing a significant improvement compared to PdAg/PtAdAg R-NSs (-0.496 V), PdAg/PtAdAg 3D-NCs (-0.425 V), and Pd/C (-0.435 V) **(Figure 8c)**. Furthermore, a similar trend in specific activities of the catalysts, obtained by normalizing their current densities to ECSA, was observed **(Figure 8d)**. Electrochemical impedance spectroscopy (EIS) spectra of the catalysts were measured in N_2-saturated 1.0 M KOH **(Figure 8f)**. Notably, PdAg/PtPdAg P-NSs exhibited a significantly lower charge transfer resistance compared to PdAg/PtAdAg R-NSs, PdAg/PtAdAg 3D-NCs, and Pd/C. This result indicates that PdAg/PtPdAg P-NSs possess a faster charge transfer rate, contributing to the enhanced EOR activity. Compared to previously reported electrocatalysts, the PdAg/PtPdAg P-NSs in this study demonstrate outstanding electrocatalytic performance in terms of mass activity.

To evaluate the stability of the PdAg/PtPdAg P-NSs, chronoamperometric (CA) curves of the PdAg/PtPdAg P-NSs, PdAg/PtPdAg R-NSs, PdAg/PtPdAg 3D-NCs, and Pd/C were obtained under the conditions of 1.0 M KOH + 1.0 M ethanol for three consecutive cycles over

a duration of 30 min **(Figure 8g)**. For CA curves, Pd/C exhibits the fastest decay in current density, while the PdAg/PtPdAg P-NSs maintain a relatively higher current density during operating reaction. The mass activity obtained from residual current density of PdAg/PtPdAg P-NSs after third cycle was 580.6 A mg^{-1}, which 1.9, 5.2, and 10.1 folds higher than that of the PdAg/PtAdAg R-NSs, PdAg/PtAdAg 3D-NCs, and Pd/C.

Given that enhanced EOR activities of the PdAg/PtPdAg P-NSs compared to those of PdAg/PtAdAg R-NSs, and PdAg/PtAdAg 3D-NCs, large number of edge and active sites coming from highly porous edges and ultrathin thickness.

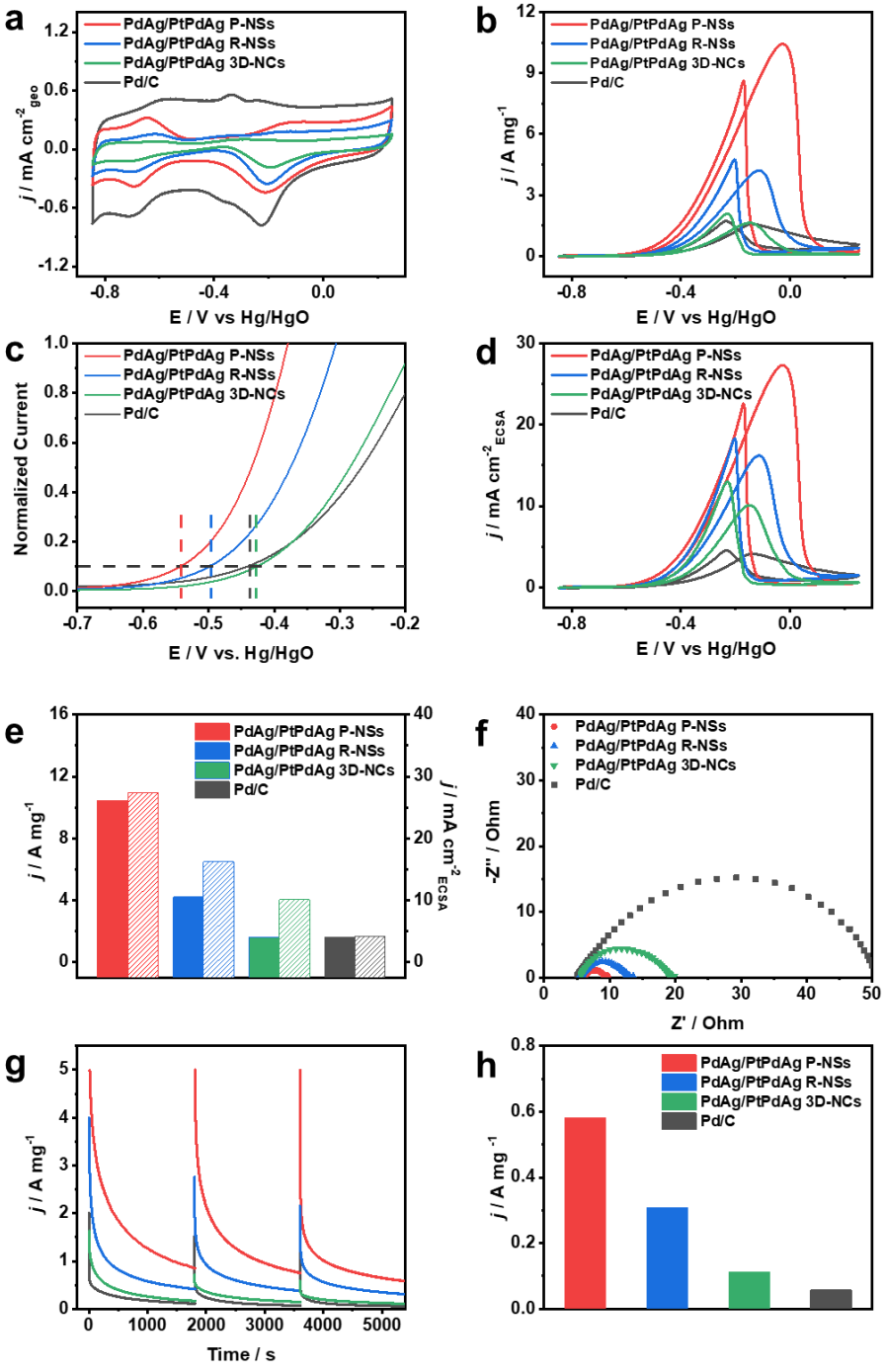

Fig. 8 CVs obtained with various catalysts in a) 1.0 M KOH, b) in 1.0 M KOH + 1.0 M ethanol. c) onset potentials of all catalysts, d) specific activities of all catalysts, e) diagram bar of mass and specific activities of the various catalysts, f) EIS curves of all catalysts in 1.0 M KOH + 1.0 M ethanol, g) chronoamperometric curves of all catalysts in N_2-saturated solutions containing 1.0 M KOH and 1.0 M ethanol at -0.08 V, and h) mass activities of all catalysts after 3rd cycle of chronoamperometric curves.

The electrochemical oxidation of ethanol generally proceeds through the C1 and/or C2 pathways, involving the carbonaceous intermediates such as $(CO)_{ads}$ and $(COCH_3)_{ads}$. [18] These carbonaceous intermediates undergo further oxidation by reaction with $(OH)_{ads}$, terminating the EOR cycle, which is generally accepted as rate-determining (RDS) in the overall process. Therefore, the adsorption and desorption behaviors of intermediate species, $(CO)_{ads}$, $(COCH_3)_{ads}$, and $(OH)_{ads}$ on the catalysts are significantly important for their EOR performance. Considering the remarkably enhanced EOR performances of the PdAg/PtPdAg P-NSs, more desirable bonding strength between reagent/intermediate species and surface of the PdAg/PtPdAg P-NSs may be formed compared to that of the other catalysts. (due to their large number of edge and active sites attributed undercoordinated atoms at highly porous edges and ultrathin thickness, as well as the optimized electronic structure and high oxophilic property influenced by alloying.) Thus, to explore the formation trend of $(OH)_{ads}$ of the catalysts, CVs were first obtained in 1.0 M ethanol + different concentrations of KOH range from 0.3 to 3.0 M. As shown in **Figure 9**, CVs exhibited that EOR activity of all catalysts gradually increased from 0.3 M to 1 M KOH concentration due to the more efficient formation of $(OH)_{ads}$ in higher KOH concentrations. [19] In contrast, further increases in KOH concentrations than 1.0 M KOH lead the decrease in EOR activity, which can be attributed to low adsorption efficiency of ethanol in excessive $(OH)_{ads}$ in higher concentrations of 1.0 M KOH. The PdAg/PtPdAg P-NSs exhibited higher activity compared to Pd/C across all KOH concentrations. In addition, ratios of the forward (I_f) and backward (I_b) peak current densities (I_f/I_b) of the PdAg/PtPdAg P-NSs were higher than those of Pd/C in all range of KOH concentrations **(Table 1)**, indicating that more facile formation of $(OH)_{ads}$ on PdAg/PtPdAg P-NSs leads less accumulation of carbonaceous intermediates on their surface, resulting in enhanced EOR activities. (Notably, compared to PdAg/PtPdAg P-NSs, higher mass activity and I_f/I_b of the PdAg/PtPdAg P-NSs can be attributed to unsaturated atoms in highly porous edges and relatively high density of Ag surface atoms with high oxophilicity to promote the formation of $(OH)_{ads}$.) Furthermore, we assessed the mass activity of various catalysts under varying ethanol concentrations to examine the trends in ethanol adsorption and the conversion of ethanol to $(CH_3CO)_{ads}$ during the EOR **(Figure 10)**. Similarly, the mass activity of the catalysts for EOR also exhibited improvement as ethanol concentration increased, attributed to the rapid adsorption of ethanol and efficient formation of $(COCH_3)_{ads}$ at higher ethanol concentrations. Notably, the mass activity of PdAg/PtPdAg P-NSs consistently outperformed that of Pd/C across all ethanol concentrations, indicating more effective ethanol adsorption and conversion to $(COCH_3)_{ads}$ in comparison to Pd/C. I_f/I_b of PdAg/PtPdAg P-NSs was also higher than that of Pd/C in all

ethanol concentrations **(Table 2)**. In comparison of Pd/C, PdAg/PtPdAg P-NSs can efficiently promote the adsorption of $(OH)_{ads}$ and $(CH_3CO)_{ads}$, which can promote electrochemical oxidation between $(OH)_{ads}$ and carbonaceous intermediates ($(CH_3CO)_{ads}$ and $(CO)_{ads}$), enhancing EOR performance.

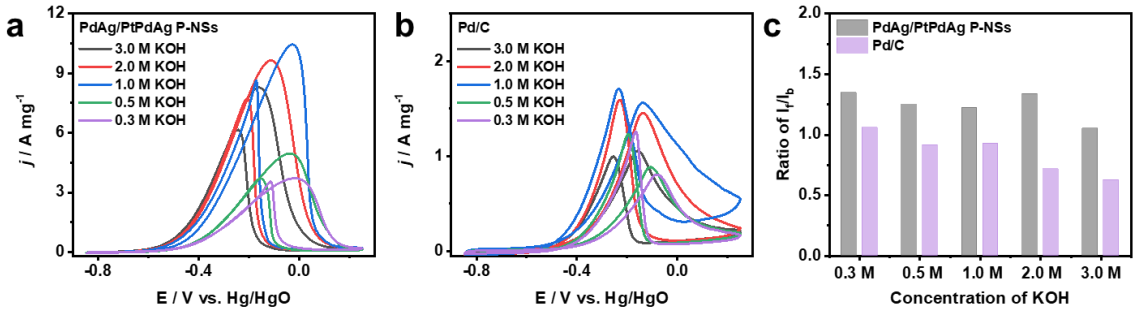

Fig. 9 Mass activities of a) PdAg/PtPdAg P-NSs and b) Pd/C in various concentration of KOH. c) I_f/I_b value of PdAg/PtPdAg P-NSs and Pd/C in various concentration of KOH.

KOH	PdAg/PtPdAg P-NSs		Pd/C	
	Mass activity (mA)	I_f/I_b	Mass activity (mA)	I_f/I_b
3.0 M	8275	1.35	1056	1.06
2.0 M	9645	1.25	1453	0.91
1.0 M	10442	1.22	1582	0.93
0.5 M	4956	1.34	884	0.72
0.3 M	3707	1.05	806	0.63

Table 1. Mass activities and I_f/I_b value of PdAg/PtPdAg P-NSs and Pd/C in different concentration of KOH.

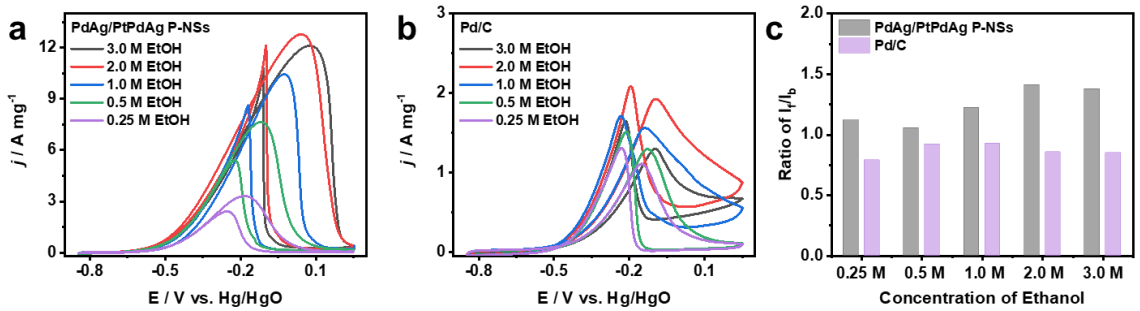

Fig. 10 Mass activities of a) PdAg/PtPdAg P-NSs and b) Pd/C in various concentration of ethanol. c) I_f/I_b value of PdAg/PtPdAg P-NSs and Pd/C in various concentration of ethanol.

EtOH	PdAg/PtPdAg P-NSs		Pd/C	
	Mass activity (mA mg^{-1})	I_f/I_b	Mass activity (mA mg^{-1})	I_f/I_b
3.0 M	12159	1.12	1299	0.79
2.0 M	12794	1.05	1924	0.92
1.0 M	10442	1.22	1582	0.93
0.5 M	7671	1.41	1294	0.86
0.25 M	3352	1.38	1109	0.85

Table 2. Mass activities and I_f/I_b value of PdAg/PtPdAg P-NSs and Pd/C in different concentration of ethanol.

To further verify the superior capability of the PdAg/PtPdAg P-NSs to remove the carbonaceous poisoning adsorbates, CO-stripping experiments were performed using different catalysts. The CO-stripping voltammograms exhibited that the PdAg/PtPdAg P-NSs are the most effective for CO oxidation **(Figure 11)**. In addition, the PdAg/PtPdAg R-NSs and PdAg/PtPdAg 3D-NCs were more efficient than the Pd/C for CO elimination. The higher CO removal abilities of trimetallic nanostructures are responsible for surface Ag atoms with high-oxophilicity, thus more Pt and Pd active sites were available for the ethanol oxidation. Notably, the relatively high density of Ag surface atoms in the PdAg/PtPdAg P-NSs effectively promotes the formation of $(OH)_{ads}$, leading to more efficient CO oxidation. Taken together, due to synergistic influence by undercoordinated atoms at highly porous edges, high atom utilization efficiency by ultrathin thickness, and pronounced oxophilicity, PdAg/PtPdAg P-NSs more efficiently promote the adsorption of $(OH)_{ads}$ and ethanol compared to other catalysts, which promotes electrochemical oxidation between $(OH)_{ads}$ and carbonaceous intermediates ($(COCH_3)_{ads}$ and $(CO)_{ads}$), enhancing EOR performance.

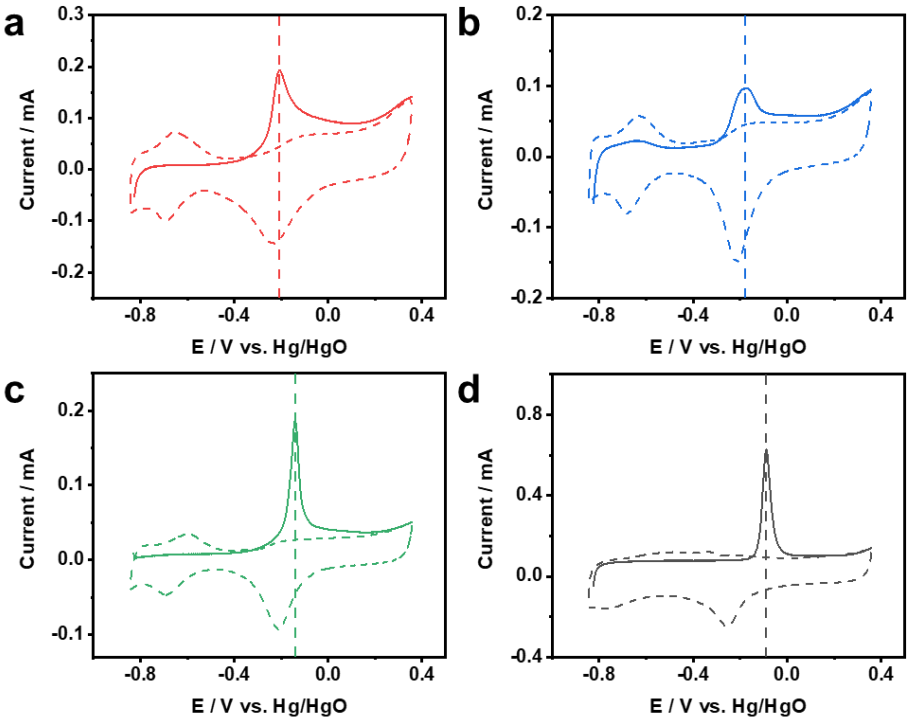

Fig. 11 a-d) CO-stripping voltammograms of PdAg/PtPdAg P-NSs, PdAg/PtPdAg R-NSs, PdAg/PtPdAg 3D-NCs, and Pd/C at a scan rate of 50 mV/s.

Catalyst	CO removal potential (V)
PdAg/PtPdAg P-NSs	-0.209
PdAg/PtPdAg R-NSs	-0.177
PdAg/PtPdAg 3D-NCs	-0.141
Pd/C	-0.090

Table 3. CO removal potential of PdAg/PtPdAg P-NSs, R-NSs, 3D-NCs, and Pd/C.

IV. Conclusion

In summary, ternary alloy ultrathin PdAg/PtPdAg P-NSs with highly porous edges are successfully synthesized by a rational aqueous synthetic method. The PdAg/PtPdAg P-NSs were synthesized by employing mild reduction conditions in absence of strong surface binding stabilizer. The PdAg/PtPdAg P-NSs has shown attractive potential for electrocatalytic activity and stability for EOR. The mass activity of PdAg/PtPdAg P-NSs was 6.6 times larger than commercial Pd/C for EOR, which can be attributed their high atom utilization efficiency attributed their ultrathin thickness and the undercoordinated atoms at the porous edges, as well as the optimized electronic structure and oxophilic property influenced by alloying. These results prove the importance of designing catalyst with controlled morphology and composition for enhancing electrocatalytic activity of catalysts. The synthesis approach and insights gained from this study could serve as a foundation for further advancements in electrocatalyst designs.

V. References

1. Monyoncho, E.A., T.K. Woo, and E.A. Baranova, *Ethanol electrooxidation reaction in alkaline media for direct ethanol fuel cells*, in *Electrochemistry*. 2018. p. 1-57.
2. Zhang, J., et al., *Cyclic Penta-Twinned Rhodium Nanobranches as Superior Catalysts for Ethanol Electro-oxidation.* J. Am. Chem. Soc., 2018. **140**(36): p. 11232-11240.
3. Lee, Y.-W., et al., *Preparation and characterization of PtIr alloy dendritic nanostructures with superior electrochemical activity and stability in oxygen reduction and ethanol oxidation reactions.* Catal. Sci. Technol., 2016. **6**(2): p. 569-576.
4. Chen, L., et al., *Shape-controlled synthesis of planar PtPb nanoplates for highly efficient methanol electro-oxidation reaction.* Chem. Commun., 2020. **56**(64): p. 9138-9141.
5. Sulaiman, J.E., et al., *Pt–Ni Octahedra as Electrocatalysts for the Ethanol Electro-Oxidation Reaction.* ACS Catal., 2017. **7**(8): p. 5134-5141.
6. Na Tian, Z.-Y.Z., Shi-Gang Sun, Yong Ding, Zhong Lin Wang, *Synthesis of Tetrahexahedral Platinum Nanocrystals with High-Index Facets and High Electro-Oxidation Activity.* Science, 2007. **316**(5825): p. 732-735.
7. Fang, C., et al., *Engineering of Hollow PdPt Nanocrystals via Reduction Kinetic Control for Their Superior Electrocatalytic Performances.* ACS Appl. Mater. Interfaces, 2018. **10**(35): p. 29543-29551.
8. Sun, Y., et al., *Interstitial Hydrogen Atom Modified PdPt Nanosheets for Efficient Ethanol Electro-oxidation with High C–C Bond Cleavage Selectivity.* ACS Appl. Energ. Mater., 2022. **5**(9): p. 10907-10914.
9. Kakade, B.A., et al., *Highly Active Bimetallic PdPt and CoPt Nanocrystals for Methanol Electro-oxidation.* J. Phys. Chem. C, 2012. **116**(13): p. 7464-7470.
10. Huang, J., et al., *PtCuNi Tetrahedra Catalysts with Tailored Surfaces for Efficient Alcohol Oxidation.* Nano Lett., 2019. **19**(8): p. 5431-5436.
11. Li, J., et al., *Ternary CoPtAu Nanoparticles as a General Catalyst for Highly Efficient Electro-oxidation of Liquid Fuels.* Angew. Chem.-Int. Edit., 2019. **58**(33): p. 11527-11533.
12. Huang, X., et al., *Freestanding palladium nanosheets with plasmonic and catalytic properties.* Nat. Nanotechnol., 2011. **6**(1): p. 28-32.
13. Hu, C., et al., *Interfacial Effects in PdAg Bimetallic Nanosheets for Selective*

Dehydrogenation of Formic Acid. ChemNanoMat, 2015. **2**(1): p. 28-32.

14. Cheong, W.-C., et al., *Free-standing palladium-nickel alloy wavy nanosheets.* Nano Res., 2016. **9**(8): p. 2244-2250.
15. Yang, L., et al., *Assembly of Alloyed PdM (Ag, Cu, and Sn) Nanosheets and Their Electrocatalytic Oxidation of Ethanol and Methanol.* Inorg. Chem., 2023. **62**(37): p. 15320-15328.
16. Hong, J.W., et al., *Ultrathin Free-Standing Ternary-Alloy Nanosheets.* Angew. Chem.-Int. Edit., 2016. **55**(8): p. 2753-8.
17. Yang, Q., et al., *Facile synthesis of ultrathin Pt–Pd nanosheets for enhanced formic acid oxidation and oxygen reduction reaction.* J. Mater. Chem. A, 2019. **7**(32): p. 18846-18851.
18. Lestarini, D.T. and J.W. Hong, *Intermetallic Pd3Pb nanobranches with low-coordinated surface atoms for highly efficient ethanol oxidation reaction.* Appl. Surf. Sci., 2023. **610**.
19. Lao, X., et al., *The ethanol oxidation reaction on bimetallic PdxAg1-x nanosheets in alkaline media and their mechanism study.* Electrochim. Acta, 2021. **374**.